IEEE Photonics Journal
An IEEE Photonics Society Publication

Open Access

Orbital Angular Momentum Shift Keying Based Optical Communication System

Volume 9, Number 2, April 2017

Caihong Kai
Pei Huang
Fei Shen
Hongping Zhou
Zhongyi Guo

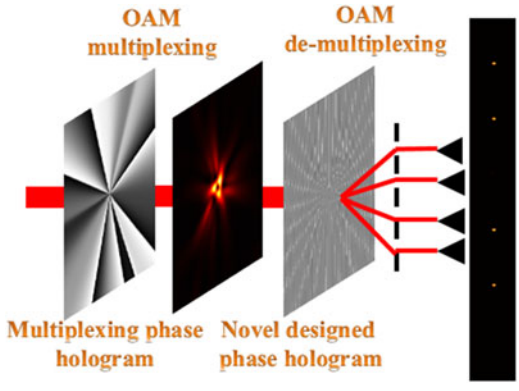

DOI: 10.1109/JPHOT.2017.2672642
1943-0655 © 2017 IEEE

IEEE photonics SOCIETY

IEEE

Orbital Angular Momentum Shift Keying Based Optical Communication System

Caihong Kai, Pei Huang, Fei Shen, Hongping Zhou, and Zhongyi Guo

School of Computer Science and Information Engineering, Hefei University of Technology, Hefei 230009, China

DOI:10.1109/JPHOT.2017.2672642

Manuscript received January 23, 2017; revised February 10, 2017; accepted February 16, 2017. Date of publication February 22, 2017; date of current version March 15, 2017. This work was supported in part by the National Natural Science Foundation of China under Grant 61575060 and Grant 61571178 and in part by the Fundamental Research Funds for the Central Universities under Grant 2015HGCH0010.
Corresponding author: Z. Guo (e-mail: guozhongyi@hfut.edu.cn).

Abstract: In the free space optical communication, the information can be encoded as the orbital angular momentum (OAM) state of light, which is called OAM shift keying (OAM-SK). This paper has proposed a communication system with OAM-SK, in which an image has been delivered from the transmitter to the receiver successfully in the simulation environment. Specifically, we have carefully designed and implemented the phase holograms used at the transmitter and the receiver for multiplexing and de-multiplexing the OAM states, respectively. At the transmitter, the multiplexing phase hologram designed by the modified Lin's algorithm is loaded on the spatial light modulator 1 (SLM1) to generate the multiplexing vortex beam, which is a superposition of multiple vortex beams with different OAM states. Correspondingly, at the receiver, a novel phase hologram is designed and loaded on the SLM2 to effectively de-multiplex the multiplexing vortex beam in different directions. In our phase hologram used at the receiver, the detected power of each OAM state can be controlled by adjusting the weight coefficient by the modified Lin's algorithm. This way, the incident power can be concentrated to the target OAM states, from which the target OAM states can be detected more effectively than conventional fork grating.

Index Terms: Optical vortices, optical communication, multiplexing phase hologram.

1. Introduction

With the development of the information technologies, there exist increasing demand for higher-speed digital communication. As a new communication technique, free space optical (FSO) communication has attracted lots of interests from researching communities, which has the advantages of both optical-fiber communication and wireless communication [1]–[3]. Moreover, the multiplexing scheme has been proposed in FSO communication system, such as time-division multiplexing (TDM) [4], wavelength-division multiplexing (WDM) [5], polarization-division multiplexing (PDM) [6], and space-division multiplexing (SDM) [7]–[14], for achieving the exponential growth of communication capacity.

Since Allen *et al.* revealed the orbital angular momentum (OAM) nature of vortex beam with helical wavefront [15], [16], the OAM has extensive applications, which has attracted increasing attentions recently [17]–[28]. The vortex beam with spiral phase structure characterized by $\exp(il\theta)$ carry the OAM of $l\hbar$, where θ is the azimuthal angle, l is the topological charge of the OAM state, and $\hbar$ is the reduced Planck constant. Both analytical and experimental results have verified the

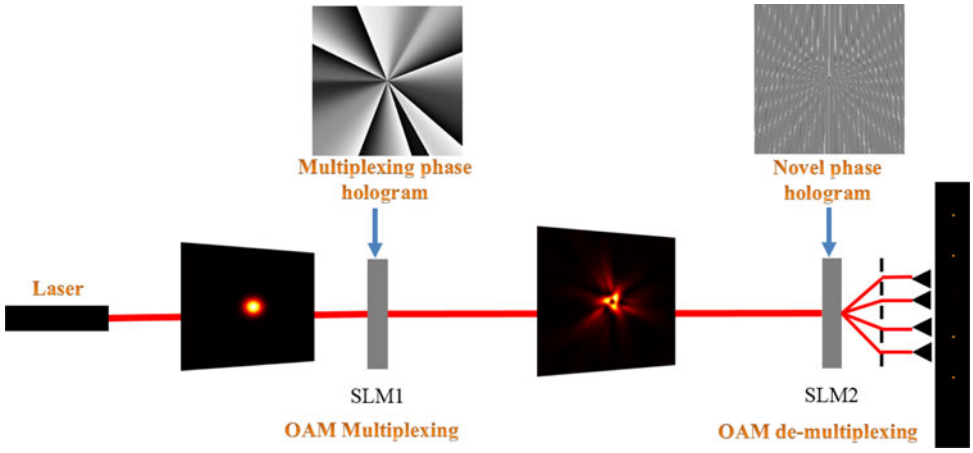

Fig. 1. Schematic diagram of the OAM-SK communication system.

feasibility of OAM multiplexing optical communication. In general, the OAM nature can be used in two ways in FSO communication: 1) OAM shift keying (OAM-SK); here, the vortex beams with different OAM states serve as encoding format, where each OAM state represents a data bit. Thus, in theory the number of data bit is also infinite [22]–[25]; 2) OAM division multiplexing (OAM-DM), where the vortex beam serves as the signal carrier, making use of the orthogonality between them, different vortex beams can be combined together to improve the communication capacity [26]–[28].

In this paper, we develop a complete FSO communication system based on OAM-SK through numerical simulation, and an image has been encoded and delivered successfully by this system. Specifically, at the transmitter, we use the modified Lin's algorithm to create the updated multiplexing phase holograms, and load them on the SLM to generate the updated multiplexing vortex beams. At the receiver, a novel phase hologram has also been designed by modified Lin's algorithm, from which both the power of each diffractive OAM state at corresponding diffraction order and the interval between diffraction orders can be controlled precisely. Finally, the concrete information can be recovered by detecting whether there exist bright spots at the center of diffraction orders. In our system, the total incident power can be almost concentrated to the target OAM states, which will decrease the energy waste and make it be more effective for detection than conventional 1-dimension fork grating. It can improve the accuracy of OAM detection and reduce the power loss than past work.

2. The Concept of FSO System Based on OAM-SK

The OAM-SK for digital modulation is a map from data bits to the OAM states. For example, by combining three vortex beams with three different OAM states as $\{+1, +2, +3\}$, the ternary code alphabet of $\{000, 001, 010, 011, 100, 101, 110, 111\}$ can be represented fully. For simplicity, assuming that the occurrences of "0" and "1" have the equal probability, each digital symbol in the code alphabet is $\log_2^{2^N}$ bit, where N is the total number of used OAM states. It is similar to the amplitude shift keying, thus, we called it the OAM shift keying. After the concrete modulation, the information can be encoded into the OAM states of the vortex beams.

To effectively transmit information based on OAM-SK, we first select a set of OAM states as a basis. Then, as shown in Fig. 1, a Gaussian beam ($l = 0$) pass through the updated multiplexing phase holograms loaded on the SLM1 to generate the multiplexing vortex beam sequence with different OAM states at the transmitter. In this way, a piece of information is encoded into the multiplexing vortex beam and transmitted to the receiver. At the receiver, we design a novel phase hologram for the chosen OAM basis, and fix it on the SLM2 as the de-multiplexer. After being de-multiplexed, the vortex beam with target OAM states will be transformed to bright spots in

corresponding diffraction orders, and other OAM states will become new values (new topological charges) accordingly. Thus, there will be bright spots at the center of corresponding diffraction orders. In order to detect the transformed bright spots, a pinhole array is laid before the detector array for filtrating the other OAM states. The detectors can obtain the digital symbol by depending on whether there exist bright spots at the specific locations. From Fig. 1, we can know that two designed phase holograms loaded on the SLM1 (at the transmitter) and SLM2 (at the receiver) are key parts of this communication system. For ensuring the high-efficiency and effective performance, we adopt an iterative algorithm to generate the updated multiplexing phase holograms at the transmitter as the encoder, and generate a fixed designed novel phase hologram at the receiver as the decoder. In the next sections we will highlight the detailed design of these phase holograms.

3. The Multiplexing Phase Holograms at the Transmitter

In the literature, there are two frequently-used methods for generating the multiplexing vortex beam with different OAM states. The simpler method is coaxial superposition by optical element [27], [28]. Another method is designing a multiplexing phase hologram based on the relationship between angular harmonic and Fourier transformation [29]–[31]. With the latter method, it is easier to control the power of each OAM state in multiplexing vortex beam and save energy in this system.

First of all, the multiplexing optical field with a set of target OAM states of $\{l_1, l_2, \cdots, l_m\}$ can be expressed as

$$B \exp\left[i\varphi(\theta)\right] = \sum_{m=1}^{n} A_{l_m} \exp\left(i l_m \theta\right) \tag{1}$$

where B is a constant modulus of amplitude, $\varphi(\theta)$ is the complex phase of multiplexing vortex beam, and $\{A_{l_m}\}$ is the weight coefficient of single vortex beam with target OAM state $\{l_m\}$. Thus, $\{|A_{l_m}|^2\}$ is the normalized power distribution of multiplexing vortex beam for different OAM states.

To generate a pure phase hologram, we expand the transmittance function $\exp\left[i\psi(\theta)\right]$ in Fourier series [29]

$$\exp\left[i\psi(\theta)\right] = \sum_{m=-\infty}^{\infty} C_m \exp\left(im\theta\right) \tag{2}$$

$$\sum_{m=-\infty}^{\infty} |C_m|^2 = 1 \tag{3}$$

where $C_m = 1/2\pi \int_0^{2\pi} \exp\left[i\psi(\theta)\right] \exp\left(-im\theta\right) d\theta$ is the complex weight coefficient in Fourier series. According to Parseval theorem, the superposition of $\{|C_m|^2\}$ is equal to 1 as shown in (3). Because of the similarity between angular harmonics and the Fourier components, m is corresponding to the OAM state of l. We can obtain the coefficients of $\{|C_{l_1}|^2, |C_{l_2}|^2, \cdots, |C_{l_n}|^2\}$ from (2), the power distribution $\{|C_{l_m}|^2\}$ can get close to the target power distribution $\{|A_{l_m}|^2\}$ by iterative algorithms and can be used to get the optimal multiplexing phase hologram $\psi(\theta)$.

To evaluate the performance of the multiplexing phase hologram $\psi(\theta)$, we define a parameter of relative root-mean-square error (R-RMSE) in (4) as a measure of how close the actual power distribution is to the target power distribution:

$$\text{R-RMSE} = \sqrt{\frac{\sum_{m=1}^{n} \left(\left|C_{l_m}\right|^2 - \left|A_{l_m}\right|^2\right)^2}{n \sum_{m=1}^{n} \left|C_{l_m}\right|^2}}. \tag{4}$$

In prior work, Lin *et al.* design an iterative algorithm and successfully generate a complex phase mask [29]. Because there still exist relative bigger deviations from the pre-set targets' power distribution, it is important to optimize the iterative algorithm for enhancing the utilization efficiency of the incident power. On this basis of Lin's algorithm, there are two important factors affecting the

final optimized result: initial weight coefficient and iteration step size. For the first one, Wang *et al.* design another iterative process to search a set of optimized initial weight coefficients and apply them to the Lin's algorithm [30]. For iteration step size, Zhu *et al.* studied how to find an optimal one and used it in Lin's algorithm [31]. From above, we can know there are two modified Lin's algorithm, which can obtain relative lower R-RMSE. In our system, the method in [31] is adopted considering both of iterative time and accuracy.

For example, the target OAM states of multiplexing phase hologram are $\{+2, +5, +8, +11\}$, and the target power distribution is averaged and normalized as $\{0.25, 0.25, 0.25, 0.25\}$. After iterative process, the obtained normalized power distribution by modified Lin's algorithm is close to the preset targets' distribution as shown in Fig. 2(a), and the phase distribution of obtained multiplexing phase hologram is shown in Fig. 2(b). On illuminating a Gaussian beam, the far-field diffraction intensity of generated multiplexing vortex beam as shown in Fig. 2(c). It is clear to see a dark core at the center, which demonstrates that the generated multiplexing vortex beam still have the vortex characteristics. According to this method, it is easier to generate the multiple vortex beam with target OAM states. It could serve as the encoder at the transmitter.

4. The Novel Phase Hologram at the Receiver

As mentioned in Section 2, the de-multiplexer is another important component in the whole communication system. The fork grating can de-multiplex the multiplexing vortex beam simultaneously. However, with increasing the diffraction order, it becomes more difficult to detect the intensity of bright spot because of the decrease of power [32], [33]. Thus, we try to design a novel phase hologram, which not only enables to de-multiplex multiple OAM states simultaneously, but also makes the detection be more effective at every diffraction orders.

Based on the principle introduced in Section 3, the modified Lin's algorithm can control the power of each OAM state in multiplexing vortex beam. Introducing the modified Lin's algorithm to the traditional fork grating, a novel phase hologram can be designed, which can concentrate incident power to the target OAM states and diffract different OAM states to different directions.

As we know, the transmittance function of conventional 1-dimension fork grating with dislocated charge of s can be written by the Fourier series [34]

$$h(\rho, \phi) = \sum_{n=-\infty}^{\infty} a_n \exp\left[in\left(s\theta + \gamma x\right)\right] \tag{5}$$

$$|a_n| = \left[\sin\left(n\pi w/d\right)\right] / \left(n\pi\right) \tag{6}$$

where a_n is the complex weight coefficient of the nth diffraction order, and $\gamma = 2\pi/d$ (d is the grating period). The space interval between adjacent diffractive vortex beams can also be adjusted by changing γ. Each component in (5) is a combination of helical phase pattern $\exp(ins\theta)$ and linear diffraction grating $\exp(in\gamma x)$. The (6) represents the normalized power distribution of the diffraction orders, and w is the grid width ($w = \frac{1}{2}d$). When a Gaussian beam illuminate to 1-dimension fork grating with the dislocated charge of s, the vortex beam with OAM state of ns appears at the nth diffraction order with the normalized power of $|a_n|^2$. When the illuminated beam is changed into a multiplexing vortex beam with a superposed OAM states of $\{l_1, l_2, \cdots, l_M\}$, the OAM state at each diffraction order becomes a new superposition of OAM states $\{ns + l_1, ns + l_2, \cdots, ns + l_M\}$. If $ns = -l_i, i \in (1, 2, \cdots, M)$, the bright spot will appear at the center of the nth diffraction order.

In general, the 1-dimension fork grating that can de-multiplex the OAM states simultaneously, can be considered as a diffractive optical element with a special transmittance function of $h(\rho, \phi)$ as shown in (5), and the power of each diffraction order depends on the weight coefficient $|a_n|^2$ in (6). The (6) is similar to a Sinc function. Thus, the incident power is almost focused on $\pm 1st$ orders. Meanwhile, the diffractive power decreases rapidly with increasing the diffraction order, which can't be controlled and will cause the energy waste in $\pm 1st$ diffraction orders. Thus, it is important to design a novel phase hologram to avoid the waste of incident energy by controlling the

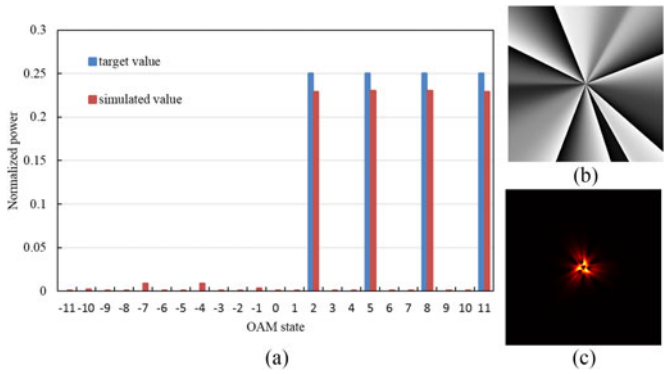

Fig. 2. Design of the multiplexing phase hologram with OAM states of $\{+2, +5, +8, +11\}$. (a) Target power distribution and simulated power distribution for different OAM states. (b) Phase distribution of the generated multiplexing phase hologram by modified Lin's algorithm. (c) Far-field diffraction intensity of the generated multiplexing vortex beam.

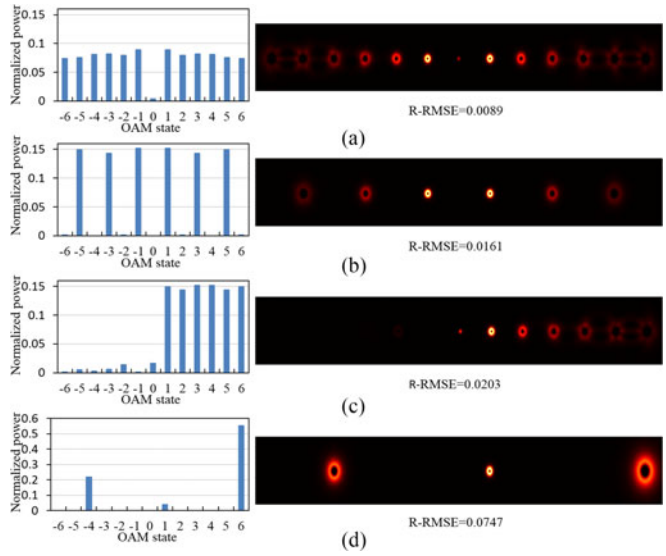

Fig. 3. Normalized power distributions and far-field diffraction results of the designed novel phase holograms with different OAM states' distributions. (a)–(c) Equal normalized power distribution for OAM states of $\{\pm 6 \pm 5 \pm 4, \pm 3, \pm 2, \pm 1\}$, $\{\pm 1, \pm 3, \pm 5\}$ and $\{+1, +2, +3, +4, +5, +6\}$ respectively. (d) Unequal normalized power distribution of $\{0.3, 0.1, 0.6\}$ for OAM states of $\{-4, +1, +6\}$.

OAM states' power distribution. According to Section 3, we add a linear phase shift for each helical phase pattern and adjust the weight coefficient a_n by the modified Lin's algorithm, which can realize the controllability of diffractive power for each OAM state.

By this way, we have designed different phase holograms with different target OAM states and power distributions. In Fig. 3, the left column is the simulated normalized power distributions of different target OAM states by modified Lin's algorithm, and right column is the corresponding far-field diffraction result by illuminating a Gaussian beam. The R-RMSE has also been calculated to quantify the evaluations between the target values and the simulated values. Fig. 3(a)–(c) show the average normalized power distribution and far-field diffraction result for OAM states of $\{\pm 6 \pm 5 \pm 4, \pm 3, \pm 2, \pm 1\}$, $\{\pm 1, \pm 3, \pm 5\}$ and $\{+1, +2, +3, +4, +5, +6\}$, respectively. As we can see, with increasing OAM state, the ring of vortex beam is becoming bigger, and the brightness of each pixel in the vortex ring is lower whereas the total power for each OAM state is constant. According

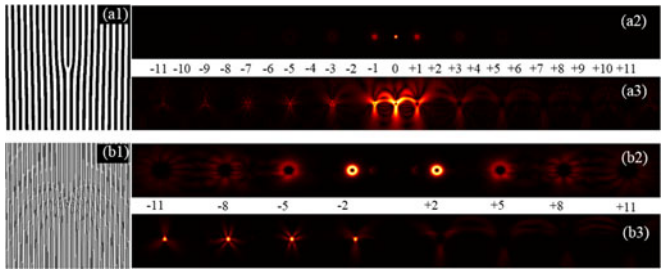

Fig. 4. Phase distributions and different far-field diffraction results of conventional 1-D fork grating (a1)–(a3) and designed novel phase hologram (b1)–(b3).

to the R-RMSE results for three-group selected OAM states as shown in Fig. 3(a)–(c), it is obvious that the more symmetrical and the more number of target OAM states with equal power, the lower R-RMSE can be obtained, which is due to the limitation of the Fourier expansion of (2). In fact, we can also observed that there exist a bright spot in the $0th$ order as depicted in Fig. 3(a) and (c), which is due to the deviation of iterative algorithm. Fig. 3(d) shows the result of diffracting power on asymmetrical-distribution OAM states of $\{-4, +1, +6\}$ with unequal normalized power distribution of $\{0.3, 0.1, 0.6\}$. From the histograms shown in Fig. 3, we can concluded that more than 80% of the incident power can be concentrated on the target OAM states. In fact, the maximum value of utilization efficiency can reach to 96% nearly. Thus, this method can reduce the energy waste efficiently.

To prove the superiority of our designed novel phase hologram, we compare its performance with that of the conventional 1-dimension fork grating. Fig. 4(a1)–(a3) show the phase distribution and the far-field diffraction of different incident beam for conventional 1-dimension fork grating. The 1-dimension fork grating only has two phases of "0" and "π" as shown in Fig. 4(a1). With illumination of the Gaussian beam, the vortex beams at $\pm 1th$ orders are easy to observe, and the others in higher diffraction orders are hard to distinguish, because the total incident power almost focus to $\pm 1th$ diffraction orders as shown in Fig. 4(a2). As a de-multiplexing device, on being illuminated by the multiplexing vortex beam with OAM states of $\{+2, +5, +8, +11\}$ generated in Section 3, the center of corresponding diffraction orders will appear bright spots. In Fig. 4(a3), there are weak bright spots in $+5th$ and $-11th$ diffractive orders, and the spot at $+5th$ order is brighter than that at $-11th$ order. Theoretically, the bright spot takes up $\frac{1}{4}|a_n|$ of total energy in the nth order. The higher diffraction order is, the weaker bright spot is obtained ($|a_n|$ will decrease with increasing the diffraction order of n). Meanwhile, the spots in $-2nd$ and $-8th$ orders can't be observed because of the concurrent result of optical interference and diffraction. The performance of the novel phase hologram with target OAM states of $\{\pm 11, \pm 8, \pm 5, \pm 2\}$ is shown in Fig. 4(b1)–(b3) for comparing with that of the conventional 1-dimension fork grating. The phase distribution of designed novel phase hologram is shown in Fig. 4(b1), which consists of complex continuous phase distribution. Fig. 4(b2) and (b3) show the far-field diffraction result with the incident Gaussian beam and the multiplexing vortex beam with OAM states of $\{+2, +5, +8, +11\}$, respectively. For the designed novel phase hologram by modified Lin's algorithm, it is easy to observe the vortex beams with target OAM states $\{\pm 11, \pm 8, \pm 5, \pm 2\}$ as shown in Fig. 4(b2). On being illuminated by the multiplexing vortex beam with OAM states of $\{+2, +5, +8, +11\}$, the designed novel phase hologram can obtain brighter spots than the conventional 1-dimension fork grating at the target diffraction orders with almost equal power as shown in Fig. 4(b3). The power of each bright spot can be calculated as $\frac{1}{4} \times \frac{1}{8}$ of total power in theory. It is higher than that of the conventional 1-dimension fork grating, except for the $\pm 1th$ orders. Thus, the designed novel phase hologram is better than 1-dimension fork grating as de-multiplexing device in the aspects of saving energy and being detected easily. For the Dammann fork grating [35], it is also not controllable for each diffraction, although it can obtain equal power distribution.

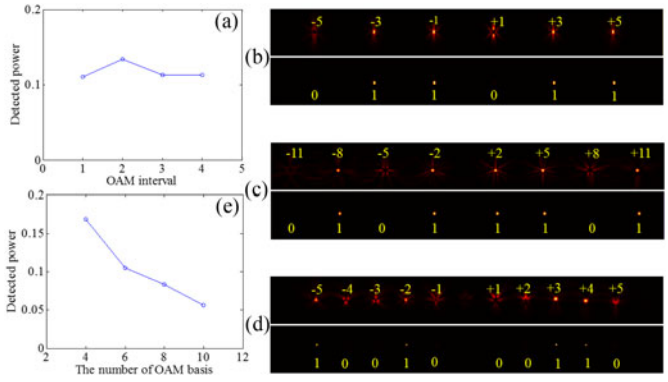

Fig. 5. (a) Performance analysis of different OAM intervals. (b), (c) De-multiplexing results and the filtrated{$\pm5, \pm3, \pm1$}, {$\pm11, \pm8, \pm5, \pm2$} and {$\pm5, \pm4, \pm3, \pm2, \pm1$} respectively. (d) Influence of OAM basis' numbers to the detected power.

5. The Image Transmission by Simulation

Before the transmission, we should select a set of OAM states as the basis firstly. Then, the designed novel phase hologram is generated by the modified Lin's algorithm based on the OAM basis which can be served as the de-multiplexing device at the receiver. In this system, the OAM basis is very important for the performance of transmission system, because the interval of OAM state has a direct influence on crosstalk between adjacent OAM states. Commonly, the larger OAM state interval is, the lower crosstalk can be obtained [28]. However, here, we could choose any set of OAM states as the OAM basis in theory. As we can see from Fig. 5(a), in our system, the OAM interval has no effect on the detection efficiency nearly in ideal environment. On the other side, the more OAM states we choose, the lower power of each OAM state is obtained. After being filtrated by a pinhole array, the bright spots might be too low to detect, as shown in Fig. 5(b)–(d).

In Fig. 5(b)–(d), the upper rows are the de-multiplexing results by the novel phase hologram with the OAM basis of {$\pm5, \pm3, \pm1$}, {$\pm11, \pm8, \pm5, \pm2$} and {$\pm5, \pm4, \pm3, \pm2, \pm1$}, respectively, and the down rows are the detected intensity after being filtrated by a pinhole array corresponding. Next, the detectors can transform the concrete intensity distribution to the corresponding digital data array. From Fig. 5(b)–(d), in the same circumstance, with increasing the number of OAM basis, the power of the filtrated bright spots will be lower. Of course, the selected pinhole size will influence the detected power of bright spots. Here, we fix the pinhole size to be square with 10×10 pixels. For describing the influence of the number of OAM basis more accurately, the detected power with different number of OAM basis can be obtained in quantification as shown in Fig. 5(e), which show that the normalized detected power of the transformed bright spots are in an inverse proportion to the number of OAM basis approximately. After consideration about the accuracy and transmission time for our communication system, we choose the OAM states of {$\pm11, \pm8, \pm5, \pm2$} as the OAM basis, as shown in Fig. 5(c).

Thus far, we can simulate a communication system based on what we described early. To verify the effectiveness of our system, we try to deliver an image in this designed system. Firstly, an image is transformed to the data flow with gray-scale value, which can be compressed into the corresponding binary data flow of "0" and "1" as shown in Fig. 6. Then, the binary data flow of the image can be divided into data groups line by line, and the data number of the group is depending on the selected OAM basis. Here, the OAM basis is chosen as {$\pm11, \pm8, \pm5, \pm2$}, therefore the data number in one group is 8. Subsequently, each data group can be mapped to a collection with corresponding OAM states, which can be transformed into the corresponding multiplexing phase holograms by the modified Lin's algorithm. Therefore, the image information can be encoded into a sequence of the updated multiplexing phase holograms. Then, a continuous Gaussian beam illuminate to the updated multiplexing phase holograms loaded on the SLM1 (at the transmitter).

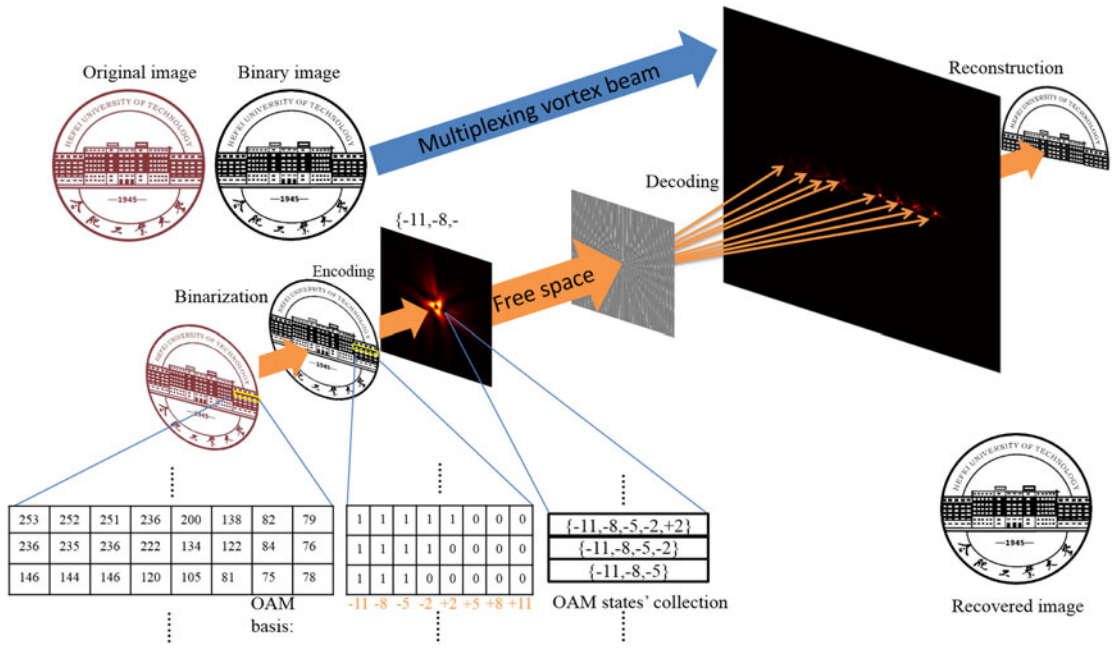

Fig. 6. Whole transmission process of OAM-SK communication system.

The multiplexing vortex beams with the binary data of image are generated and delivered to the receiver from free space.

At the receiver, the multiplexing vortex beam can be de-multiplexed by the novel phase hologram fixed on the SLM2. The target OAM states will be converted to bright spots, and they will appear at the center of corresponding diffraction orders. After being filtrated by a pinhole array, the detector array can confirm the binary data at each pixel, depending on whether there is a bright spot at the corresponding location. Then, the binary data is rearranged at the corresponding pixel. In our simulation, we select the OAM states of $\{\pm 11, \pm 8, \pm 5, \pm 2\}$ as the basis. When the multiplexing vortex beam with OAM states of $\{-11, -5, -2, +2, +8\}$ is de-multiplexed by the designed phase hologram, the diffractive result and the filtrated result by a pinhole array can be found in Fig. 5(c), and the detector will transform the intensity distribution to the binary data of "01011101" accordingly. Keeping the transmission loop, the selected image can be delivered from the transmitter to the receiver successfully. Then, the obtained binary data can be rearranged to recover the original binary image. The whole transmission process of system is shown in Fig. 6. In our simulated results, we successfully deliver an image with 536×536 pixels. At the receiver, the recovered image has a high fidelity to the binary image if we choose an appropriate pinhole size. It verifies the feasibility of our system.

In our system, the high-efficiency methods of OAM multiplexing and de-multiplexing are adopted, which will improve the system performance and reduce error. Although the received image is not perfect, because only binary data flow can be delivered. These OAM multiplexing and de-multiplexing methods have great potential to be applied to the optical communication based on OAM to improve the channel capacity and spectral efficiency. In addition to this, the transmitting speed will be limited by the update frequency of the multiplexing phase hologram at the transmitter (SLM1). The higher update frequency of SLM can reach, the higher transmitting speed can be obtained. In the future, we will also try to optimize the OAM-SK communication system to deliver the kromogram with low error and improve the applicability of system.

6. Conclusion

We have proposed a free space communication system based on OAM-SK. At the transmitter, with the aid of the spatial light modulator, the multiplexing vortex beam can be easily generated by multiplexing phase hologram, and, at the receiver, we design a novel phase hologram by controlling the power distribution of each OAM state, in which the incident power on the unnecessary diffraction orders can be reduced greatly. Both of the multiplexing phase hologram (at the transmitter) and the novel phase hologram (at the receiver) have been optimized by the modified Lin's algorithm. Based on our scheme, an image is encoded by a set of OAM states at the transmitter and decoded at the receiver after free space transmission. and the recovered image shows a high fidelity to the original image, which show the correctness and the effectiveness of our system.

References

[1] V. W. Chan, "Free-space optical communications," *J. Lightw. Technol.*, vol. 24, no. 12, pp. 4750–4762, Dec. 2006.
[2] X. Zhu and J. M. Kahn, "Free-space optical communication through atmospheric turbulence channels," *IEEE Trans. Commun.*, vol. 50, no. 8, pp. 1293–1300, Aug. 2002.
[3] K. Kiasaleh, "Performance of coherent DPSK free-space optical communication systems in k-distributed turbulence," *IEEE Trans. Commun.*, vol. 54, no. 4, pp. 604–607, Apr. 2006.
[4] T. Richter *et al.*, "Transmission of single-channel 16-QAM data signals at terabaud symbol rates," *J. Lightw. Technol.*, vol. 30, no. 4, pp. 504–511, Feb. 2012.
[5] A. Gnauck, P. Winzer, S. Chandrasekhar, X. Liu, B. Zhu, and D. Peckham, "Spectrally efficient long-haul WDM transmission using 224-gb/s polarization-multiplexed 16-QAM," *J. Lightw. Technol.*, vol. 29, no. 4, pp. 373–377, Feb. 2011.
[6] X. Zhou *et al.*, "64-tb/s, 8 b/s/hz, PDM-36QAM transmission over 320 km using both pre-and post-transmission digital signal processing," *J. Lightw. Technol.*, vol. 29, no. 4, pp. 571–577, Feb. 2011.
[7] G. Milione *et al.*, "4 $\times$ 20 gbit/s mode division multiplexing over free space using vector modes and a q-plate mode (de) multiplexer," *Opt. Lett.*, vol. 40, no. 9, pp. 1980–1983, 2015.
[8] G. Milione, E. Ip, M. J. Li, J. Stone, G. Peng, and T. Wang, "Mode crosstalk matrix measurement of a 1 km elliptical core few-mode optical fiber," *Opt. Lett.*, vol. 41, no. 12, p. 2755, 2016.
[9] E. Ip *et al.*, "SDM transmission of real-time 10 gbe traffic using commercial SFP + transceivers over 0.5 km elliptical-core few-mode fiber," *Opt. Exp.*, vol. 23, no. 13, p. 17120, 2015.
[10] G. Milione, D. A. Nolan, and R. R. Alfano, "Determining principal modes in a multimode optical fiber using the mode dependent signal delay method," *J. Opt. Soc. Amer. B*, vol. 32, no. 1, pp. 143–149, 2015.
[11] R. R. Alfano, G. Milione, E. J. Galvez, and L. Shi, "Optical sources: A laser for complex spatial modes," *Nature Photon.*, vol. 10, no. 5, pp. 286–288, 2016.
[12] X. Liu *et al.*, "1.12-tb/s 32-QAM-OFDM superchannel with 8.6-b/s/hz intrachannel spectral efficiency and space-division multiplexed transmission with 60-b/s/hz aggregate spectral efficiency," *Opt. Exp.*, vol. 19, no. 26, pp. B958–B964, 2011.
[13] G. Milione, T. A. Nguyen, J. Leach, D. A. Nolan, and R. R. Alfano, "Using the nonseparability of vector beams to encode information for optical communication," *Opt. Lett.*, vol. 40, no. 21, pp. 4887–4890, 2015.
[14] R. Ryf *et al.*, "Mode-division multiplexing over 96 km of few-mode fiber using coherent 6 $\times$ 6 MIMO processing," *J. Lightw. Technol.*, vol. 30, no. 4, pp. 521–531, Feb. 2012.
[15] A. M. Yao and M. J. Padgett, "Orbital angular momentum: Origins, behavior and applications," *Adv. Opt. Photon.*, vol. 3, no. 2, pp. 161–204, 2011.
[16] A. E. Willner *et al.*, "Optical communications using orbital angular momentum beams," *Adv. Opt. Photon.*, vol. 7, no. 1, pp. 66–106, 2015.
[17] N. Cvijetic, G. Milione, E. Ip, and T. Wang, "Detecting lateral motion using lights orbital angular momentum," *Sci. Rep.*, vol. 5, 2015, Art. no. 15422.
[18] Z. Guo, S. Qu, and S. Liu, "Generating optical vortex with computer-generated hologram fabricated inside glass by femtosecond laser pulses," *Opt. Commun.*, vol. 273, no. 1, pp. 286–289, 2007.
[19] Z. Guo, S. Qu, Z. Sun, and S. Liu, "Superposition of orbit angular momentum of photons by combined computer-generated hologram fabricated in silica glass with femtosecond laser pulses," *Chin. Phys. B*, vol. 17, no. 11, pp. 4199–4205, 2008.
[20] L. Zhu *et al.*, "Calculating the torque of the optical vortex tweezer to the ellipsoidal micro-particles," *Opt. Commun.*, vol. 354, pp. 34–39, 2015.
[21] J. Zhang *et al.*, "Circular polarization analyzer based on an archimedean nano-pinholes array," *Opt. Exp.*, vol. 23, no. 23, pp. 30523–30531, 2015.
[22] Z. Bouchal and R. Celechovsk, "Mixed vortex states of light as information carriers," *New J. Phys.*, vol. 6, no. 1, 2004, Art. no. 131.
[23] D. Zhang, X. Feng, and Y. Huang, "Encoding and decoding of orbital angular momentum for wireless optical interconnects on chip," *Opt. Exp.*, vol. 20, no. 24, pp. 26986–26995, 2012.
[24] G. Gibson *et al.*, "Free-space information transfer using light beams carrying orbital angular momentum," *Opt. Exp.*, vol. 12, no. 22, pp. 5448–5456, 2004.
[25] M. Krenn *et al.*, "Communication with spatially modulated light through turbulent air across vienna," *New J. Phys.*, vol. 16, no. 11, 2014, Art. no. 113028.

[26] H. Huang *et al.*, "Mode division multiplexing using an orbital angular momentum mode sorter and MIMO-DSP over a graded-index few-mode optical fibre," *Sci. Rep.*, vol. 5, 2015, Art. no. 14931.
[27] J. Wang *et al.*, "Terabit free-space data transmission employing orbital angular momentum multiplexing," *Nature Photon.*, vol. 6, no. 7, pp. 488–496, 2012.
[28] S. Li and J. Wang, "Performance evaluation of analog signal transmission in an orbital angular momentum multiplexing system," *Opt. Lett.*, vol. 40, no. 5, pp. 760–763, 2015.
[29] J. Lin, X. Yuan, S. H. Tao, and R. E. Burge, "Synthesis of multiple collinear helical modes generated by a phase-only element," *J. Opt. Soc. Amer. A*, vol. 23, no. 5, pp. 1214–1218, 2006.
[30] L. Zhu and J. Wang, "Simultaneous generation of multiple orbital angular momentum (OAM) modes using a single phase-only element," *Opt. Exp.*, vol. 23, no. 20, pp. 26221–26233, 2015.
[31] Y. Zhu, K. Zou, Z. Zheng, and F. Zhang, "1 $\lambda\times$ 1.44 tb/s free-space IM-DD transmission employing OAM multiplexing and PDM," *Opt. Exp.*, vol. 24, no. 4, pp. 3967–3980, 2016.
[32] I. Moreno, J. A. Davis, B. M. L. Pascoguin, M. J. Mitry, and D. M. Cottrell, "Vortex sensing diffraction gratings," *Opt. Lett.*, vol. 34, no. 19, pp. 2927–2929, 2009.
[33] I. Gibson, J. Courtial, M. Vasnetsov, S. Barnett, S. Franke-Arnold, and M. Padgett, "Increasing the data density of free-space optical communications using orbital angular momentum," *Proc. SPIE*, vol. 5550, 2004, pp. 367–373.
[34] Z. Wang, N. Zhang, and X.-C. Yuan, "High-volume optical vortex multiplexing and de-multiplexing for free-space optical communication," *Opt. Exp.*, vol. 19, no. 2, pp. 482–492, 2011.
[35] N. Zhang, X. Yuan, and R. Burge, "Extending the detection range of optical vortices by dammann vortex gratings," *Opt. Lett.*, vol. 35, no. 20, pp. 3495–3497, 2010.